scientific reports

Check for updates

OPEN

Aptamer-enhanced ultrasensitive electrochemical detection of HER-2 in breast cancer diagnosis using ZnO tetrapod-K_4PTC nanohybrids

Reema Rawat[1], Souradeep Roy[1], Tapas Goswami[2], Fatemeh Sadat Mirsafi[3], Mustafa Ismael[4], Till Leissner[3], Yogendra Kumar Mishra[3], James McLaughlin[5], Krishna Kant[6,7]✉ & Ashish Mathur[8]✉

Breast cancer continues to be a severe global health issue, emphasizing the critical need for accurate and timely detection and screening of large numbers of patients. This ailment places an enormous strain on healthcare resources and poses severe mortality risks for women globally if not addressed promptly. Conventional diagnostic techniques face obstacles such as expensive apparatus, intricate procedures, and long duration in stratification. Therefore, the development of point-of-care (PoC) devices that enable early detection of breast cancer is of utmost importance. This research article focuses on the development of an electrochemical based aptasensor for the detection of Human Epidermal Growth Factor Receptor 2 (HER-2) using the novel nanohybrid substrate material, which consists of a 3D Zinc Oxide Tetrapods (ZnOT) and Potassium Perylene Tetra Carboxylate (K_4PTC). The analytical performance of the bio-nanoelectrode for detecting HER-2 was assessed using Square Wave Voltammetry (SWV) analysis. The developed nano-biosensor exhibited linear response in the range from 1 fg/mL – 10 µg/mL, and the overall limit of detection and sensitivity of the developed sensor is observed around 0.58 fg/mL and 2.08 µA/fg/mL/mm^2, respectively. The shelf life of the sensor substrate is above one month in normal storage conditions. This study offers a base for the development of an efficient and sensitive breast cancer biomarker sensing platform, which has the potential to be implemented at a low cost for society and perform screening testing for breast cancer management in rural areas.

Keywords Breast cancer, HER-2, Electrochemical biosensor, ZnOT-K_4PTC nanohybrids, Affordable healthcare, Early detection

Breast cancer is the most common category of cancer and the second leading root of mortality among the female populace. An estimated 2.1 to 2.3 million women worldwide are affected by it annually[1]. There were 1 million deaths globally, it is projected that the number of breast cancer cases is projected to increase by many times 2025 [2]. HER-2 is a common biomarker for breast cancer. It is overexpressed in 20–30% of breast cancer cells and has emerged as an essential biomarker for guiding therapeutic decisions in breast cancer patients[3,4]. Therefore, timely and accurate detection of breast cancer, especially in cases containing HER-2 overexpression, is crucial for adopting efficient therapeutic strategies.

Primary screening is important for valuable treatment of breast cancer which may result in improved survival rates. Several methods, such as mammography, sonography, thermography, positron emission tomography (PET), molecular breast imaging, magnetic resonance imaging (MRI, biopsy, and computed tomography (CT) scans, are utilized for breast cancer screening[5–7]. Traditional methods for HER-2 detections contain enzyme-linked immunosorbent assays, radioimmunoassays, electrochemical immunoassays, and colorimetric

[1]Department of Allied Health Sciences, School of Health Sciences and Technology, UPES, Dehradun, India. [2]Department of Chemistry, School of Advanced Engineering, UPES, Dehradun, India. [3]Mads Clausen Institute, University of Southern Denmark, NanoSYD, Sønderborg, Denmark. [4]Middle Technical University, Al-Za'faraniyah, St. 54, Baghdad, Iraq. [5]School of Engineering, Ulster University, Belfast, UK. [6]CINBIO, Universidade de Vigo, Campus Universitario As Lagoas Marcosende, Vigo 36310, Spain. [7]Department of Biotechnology, School of Engineering and Applied Sciences, Bennett University, Greater Noida, UP, India. [8]Centre for Interdisciplinary Research and Innovation (CIDRI), UPES, Dehradun, India. ✉email: Krishna.kant@uvigo.gal; ashish.mathur@ddn.upes.ac.in

immunoassays[8] these tests are recommended for patients exhibiting signs of cancer, typically at the later stages on the disease onset, where recovery becomes more challenging. Furthermore, conventional techniques, require complex handling and expert operating personal for analysing the data and sample. Furthermore, the poor availability of these facilities and related high cost makes it difficult to bear for low socio-economic countries. These hurdles, emphasizing the need to develop alternative methods capable of mitigating these limitations and provide efficient solutions for early diagnosis of cancer. Enhancing the accessibility and efficacy of HER-2 determination necessitates a more streamlined, screening for female population. The patients with breast cancer show elevated concentrations of HER-2 in their blood, ranging from 15 ng/mL to 75 ng/mL, in direct contrast to the levels observed in healthy individuals, usually between 2 ng/mL and <15 ng/mL[9]. Electroanalytical transduction application in biosensors has garnered significant attention due to several advantageous properties like cost-effectiveness sensitivity, and efficient miniaturization for appropriate point-of-care services[10–15].

The integration of appropriate nanomaterials enhances the electroanalytical characteristics when used as bioelectrode modifiers to develop electrochemical biosensors. The benefits of using nanomaterials include an increased surface-to-volume ratio, which leads to better receptor immobilization, and quantum confinement effects, which contribute to enhanced electronic conductivity or signal amplification[16,17]. The fabrication of electrochemical biosensors and bioelectrodes involves precise engineering to ensure optimal performance, integrating advanced materials with innovative design techniques. In comparison to 0D, 1D, and 2D nanomaterials, which have simpler morphologies, 3D nanostructures typically combine various nanoscale features within a single structure. These 3D nanomaterials offer a highly electroactive surface area, making them more effective at targeting analytes of interest, amplifying signals, and performing efficient biosensing[18].

ZnO nanostructures have been successfully synthesized in the 3D tetrapodal morphology, offering a versatile platform for multipurpose applications[19,20]. A study reported by Sulciute et al. highlighted the higher charge transfer kinetics at ZnO tetrapodal (ZnOT) surfaces in comparison with dots and ribbons morphology[21]. This development was assigned to reduced carrier scattering events, resulting from fewer interfaces at interparticle junctions. Additionally, the 3D morphology of ZnOTs offers an elevated active surface area, allowing efficient surface functionalization, improved electrochemical capacitance, and better electron transfer kinetics[22,23]. Potassium perylene-3, 4, 9, 10-tetracarboxylate potassium salt (K_4PTC) has gained particular interest due to its high solubility in water and solution processability. It is observed that the carboxylate groups present in K_4PTC enhance the electrochemical activity by several folds. The electrochemical oxidation of R-COO groups, commonly known as the Kolbe reaction, is one of the most well-known and primary electro-organic reactions)[24].

During the past two decades, aptamers have been evaluated against different targets[25]. In principle, aptamers with high specificity and affinity can be chosen in vitro for any target, including tiny molecules, peptides, proteins, and complete organisms[26]. This comprehensive target identification ability makes them promising probes capable of competing with biomolecules to detect various diagnostically significant analytes. Biosensors that, combined with aptamers, provide a competitive edge over those that rely on natural receptors like antibodies, enzymes, and peptides[27]. The characteristic properties of HER-2 make it suitable biomarker. It is a 185 kDa transmembrane receptor that belongs to the tyrosine kinase family, specifically within the epidermal growth factor receptor group. It is present in a variety of tissues, including epithelial, mesenchymal, and neuronal cells, where it responds to signals promoting cell growth. Normally, the activation of HER-2 is regulated by the presence of its ligands, which are part of the epidermal growth factor family. However, when HER-2 is overexpressed, it leads to continuous activation of growth signals, a major cause in the development of breast cancer. Due to this, HER-2 serves as a crucial biomarker for diagnosing and predicting early-stage breast cancer outcomes, contributing to improved survival rates and treatment success in patients[28].

In this work, ZnO tetrapod-K_4PTC (ZnOT-K_4PTC) nanohybrids was used for electroanalytical aptasensing of breast cancer using HER-2 concentrations. The novel nanohybrid structure primarily consists of ZnO tetrapod cores encased by K_4PTC molecules, forming a unique core-shell structure. The K_4PTC layer, which is rich in carboxylate groups, is crucial for aptasensing because it enables precise binding interactions with aptamer molecules that target HER-2 aptamer. The ZnO tetrapod cores boost the electronic conductivity of the sensing platform, facilitating efficient charge transfer and enabling the sensitive detection of HER-2. This research represents an innovative method for the detection of HER-2, an essential biomarker. In contrast to prior stabilised and published approaches from our research group, the fabrication and application of active nanohybrids onto a carbon screen-printed electrode, which functions as a layer of electro-active transducers[29,30]. the presented work has the novelty of applying very first time a nanohybrid substrate made up of ZnOT nanostructures with K_4PTC, A thorough analysis was conducted to determine the structural, chemical, and electrochemical properties of this configuration, to confirm the successful synthesis of nanohybrid. Our synthesized nanohybrid demonstrates exceptional sensing capabilities when exposed to HER-2 oxidations in Methylene Blue-containing Phosphate-Buffered Saline (PBS-MB), a choice justified by Methylene Blue's role as a redox mediator, enhancing electron transfer during the sensing process. The observed increased activity was higher than that of pure ZnOT and K_4PTC in isolation. Consequently, in serum and (PBS-MB) samples, our nanohybrid material exhibited exceptionally high sensitivity and a significantly LoD for HER-2. All methods were conducted in accordance with relevant guidelines and regulations, and ethical approval for the study was obtained and documented as per the requirements.

Results and discussion

Material surface characterization

XRD

The presented Fig. 1a obtained using the (D8 ADVANCE ECO-Bruker) shows the XRD pattern of ZnOT-K_4PTC nanohybrids, instrument. The absence of any diffraction peaks corresponding to residual zinc or other suboxides in the spectrum confirms the formation of homogenous, pure, and well-crystallized ZnOT, as evidenced by

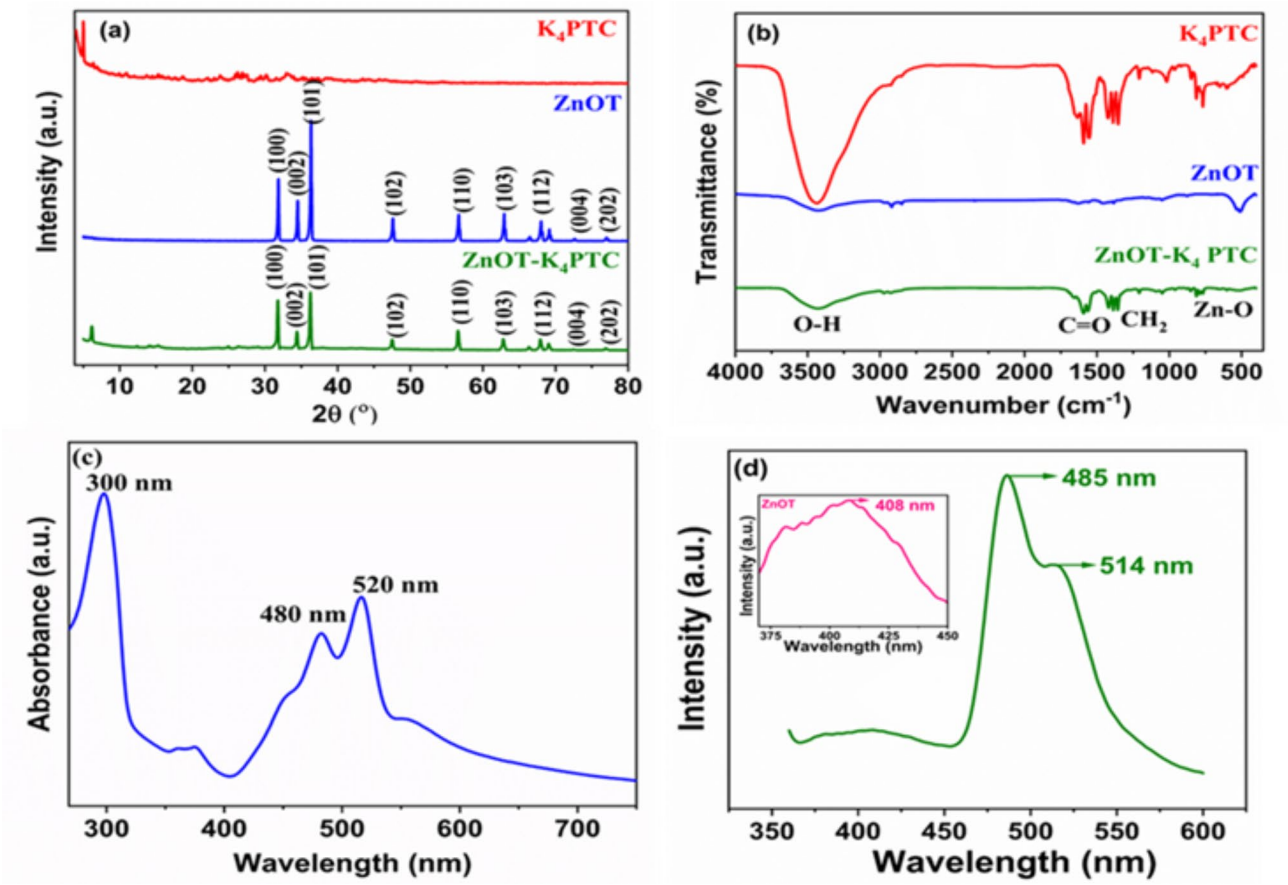

Fig. 1. (**a**) XRD plot within the range of 2θ = 8° – 80° (**b**) FTIR spectra recorded within the range of 4000–450 cm^{-1} (**c**) UV-VIS spectrum of ZnOT-K_4PTC within the range of 265–800 nm (**d**) PL Spectra of ZnOT-K_4PTC and ZnOT and K_4PTC exhibit emission spectra within the range of 300 to 500 nm (Insite).

all the discernible diffraction peaks[31]. Notably, the XRD pattern features a particularly prominent peak for ZnOT at 2θ = 36.45°, corresponding to the (101) plane. This is evidenced by the (101) being the most favourable orientation for the nucleation and growth of ZnOT crystals[31]. The prominent peak at 2θ = 6° and the smaller peaks at 2θ = 12.40° and 27.30° are attributed to the distinction phases of K_4PTC[30] Further analysis using the Scherrer Eq. (1) [32]:

$$D = \frac{0.9\lambda}{\beta \cos\theta} \tag{1}$$

The parameter 'β' signifies the broadening of the diffraction peak measured at half its maximum intensity, expressed in radians. Conversely, 'D' represents the grain size of the material. The symbol 'λ' denotes the wavelength of the X-ray radiation, while 'θ' stands for the Bragg angle, which is the angle of incidence, reveals the grain size for ZnOT is approximately 38.30 nm, for K_4PTC is 1.2 nm, and for the ZnOT-K_4PTC nanohybrid is approximately 15.96 nm. The significant reduction in grain size for the nanohybrid is attributed to the interaction between ZnOT and K_4PTC phases. The crystalline nature of ZnOT is well-supported by the sharp and intense diffraction peaks observed in its XRD pattern, indicating high crystallinity. However, introducing K_4PTC phases into the nanohybrid leads to a slight broadening of peaks, suggesting a reduced crystalline domain size. This reduction is likely due to the integration of the amorphous or semi-crystalline K_4PTC phase, which disrupts the periodic lattice of ZnOT, resulting in smaller crystalline regions in the composite. Such structural changes contribute to the unique properties of the nanohybrid material.

FTIR

The FTIR spectrum obtained using the Frontier FT-IR/FIR instrument (Perkin Elmer) is shown in (Fig. 1(b) and displays a distinct peak at 3445 cm^{-1}, signifying the existence of -OH stretching vibrations. This peak reflects hydroxyl groups associated with alcohols, phenols, or adsorbed water molecules. Additionally, the peak at 2923 cm^{-1} corresponds to CH_2 stretching vibrations, indicating the presence of aliphatic chains in the hybrid material. The spectrum reveals a peak at 509 cm^{-1}, which is a clear indicator of Zn-O stretching vibrations, characteristic of the structural composition of the material[33]. The spectrum also shows a notable peak at approximately 1623 cm^{-1}, ascribed to the C = O stretching vibrations of the carboxylate acid groups in K_4PTC.

A smaller peak at 1384 cm^{-1}, representing symmetric stretching of the carboxylate groups, further confirms the coordination environment in the hybrid. Further peaks at 1579 cm^{-1} and 1595 cm^{-1} indicate the aromatic C-C stretching vibrations inherent to K_4PTC[34]. The band near 1120 cm^{-1} is attributed to the C-O stretching vibrations, highlighting ether or ester groups within the material's matrix. A weak absorption near 890 cm^{-1} suggests the presence of out-of-plane bending vibrations associated with aromatic rings, providing additional structural insights. The examined shift in the peak within the FTIR spectrum of the nanohybrid suggests a potential π-π stacking interaction between the pyrenyl group of K_4PTC[30] and the ZnOT nanosheet, highlighting the complex interplay of molecular forces and interactions within the nanohybrid structure. The ZnOT-K_4PTC hybrid, in its as-prepared state, demonstrated discernible absorption peaks, which suggest its hybrid characteristics. This includes vibrational modes related to molecular interactions, such as hydrogen bonding, metal-ligand coordination, and π-π stacking. These features highlight the material's potential applicability in biosensing due to its ability to facilitate selective molecular recognition and signal transduction.

UV-Vis and photoluminescence

The Spectro Photo meter UV-Vis (LAMDA 35, Perkin Elmer) and Photoluminescence Spectrophotometer (LAMDA 45, Perkin Elmer) were used to analyze the optical properties of the synthesized nanohybrid. The absorption spectrum in Fig. 1c exhibits distinct peaks between 480 nm and 520 nm[34–36], corresponding to K_4PTC. These peaks are characteristic of the π–π transitions in K_4PTC molecules, further confirming their incorporation into the nanohybrid structure. The prominent peak at around 300 nm also signifies ZnOT[37]. This absorption band is associated with the electronic transitions within the ZnO structure, particularly the intrinsic bandgap transitions, indicating the presence of ZnOT as a key component. A photoluminescence (PL) spectrum (Fig. 1d indicates the presence of ZnOT and K_4PTC. PL spectra provide complementary insights into the optical activity of the nanohybrid, capturing emission phenomena that correlate with the observed absorption bands. The ZnOT and K_4PTC exhibit emission spectra within the range of 300 to 500 nm as presented in inset of Fig. 1d. This emission range reflects the radiative recombination of charge carriers within the ZnOT and K_4PTC components, suggesting effective interaction between the materials. In our synthesized nanohybrid, the presence of K_4PTC was indicated by the bands at 485 and 514 nm[34]. These specific peaks are well-aligned with the known luminescent properties of K_4PTC, confirming its role as a luminescent center within the hybrid matrix. The slight bump shown at 408 nm signifies the presence of ZnOT[38,39]. This feature indicates defect-related emissions in ZnO, such as oxygen vacancies or zinc interstitials, commonly observed in ZnOT-based materials. These PL spectra closely matched the absorption band of the nanohybrid, which confirms the effective synthesis of the ZnOT-K_4PTC nanohybrid. The overlap between absorption and emission spectra underscores the successful coupling of the two components, validating the integrity and functionality of the synthesized material.

SEM micrograph

The Field Emission Scanning Electron Microscopy analysis was performed using the (FESEM, *ZEISS*) instrument. which revealed that tetrapods contain four arms branching from the same center and that the angles amongst the arms are approximately similar[40,41] with a coating of functionalized K_4PTC, as depicted in Fig. 2a, b,c. This characteristic tetrapod structure, symmetrical branching, is a hallmark of ZnOT materials and suggests controlled synthesis conditions. The arms are uniform in length and diameter, further validating the fabrication process's consistency and reproducibility. Additionally, the coating of K_4PTC is observed as a uniform layer around the ZnOT tetrapods, enhancing their surface properties and enabling potential functional applications. Such coating provides opportunities for improved interaction with light and charge transport in hybrid materials. The Energy Dispersive X-ray Spectroscopy (EDAX) analysis revealed that zinc is present in 74 wt % in the synthesized nanohybrid, followed by carbon, potassium, and oxygen in 14 wt, 7.90 wt, and 3 wt% respectively as shown in Fig. 2d. The high zinc content indicates that ZnOT constitutes the core structural component of the nanohybrid. The presence of carbon and potassium validates the effective incorporation of K_4PTC, while the oxygen content aligns with the ZnOT matrix and functional groups from the K_4PTC. The uniform elemental distribution observed in EDAX further supports the successful synthesis of the ZnOT-K_4PTC nanohybrid. These findings confirm the effective structural and compositional integration of ZnOT and K_4PTC into a hybrid material with enhanced functional capabilities.

X-ray photoelectron spectroscopy (XPS) of ZnOT-K4PTC nanohybrid

The XPS spectrum of the ZnOT-K_4PTC nanohybrid, obtained using a PHI5000 Versa Probe II (ULVAC-PHI, Japan), is shown in Fig. 3a. It reveals four dominant elements, namely Zn2p, O1s, C1s, and K2p. The XPS spectrum is associated with the core-level regions of Zn 2p. At approximately 1021.6 eV and 1045 eV, the ZnOT-K_4PTC nanohybrid exhibited a doublet, corresponding to the Zn's 2p3/2 and 2p1/2 core levels, respectively[42]. This distinct doublet separation signifies a stable zinc oxidation state in the hybrid material, reinforcing the reliability of ZnO formation. 23.4 eV is the difference in binding energy between the two lines, which is well within the ZnO standard reference value. The first peak observed in the oxygen-deficient ZnO matrix is ascribed to Zn2 + ions. Additionally, each Zn 2p3/2 XPS peak is distinct. Therefore, it can be verified that the predominant form of zinc ions present on the surfaces of the samples is Zn2 + [43]. This evidence confirms that ZnO forms in the hybrids in the as-synthesized state. The O1s spectra in Fig. 3b display notable peaks at 531, 533, and 534 eV, corresponding to distinct oxygen-containing functional groups and chemical environments. At 531 eV, the peak primarily represents oxygen bound in C-O groups. In comparison, the peaks at 533 eV and 534 eV are attributed to hydroxyl groups and carboxylic groups, respectively. These assignments provide insights into the functionalization of the nanohybrid. The presence of oxygen atoms bonded to carbon via carbon-oxygen (C-O) single bonds is indicated by the peak at 531 eV. The observed peak can be attributed to chemical species with C-O linkages, including ethers, alcohols, or other organic compounds. The identification of a peak at 533 eV signifies

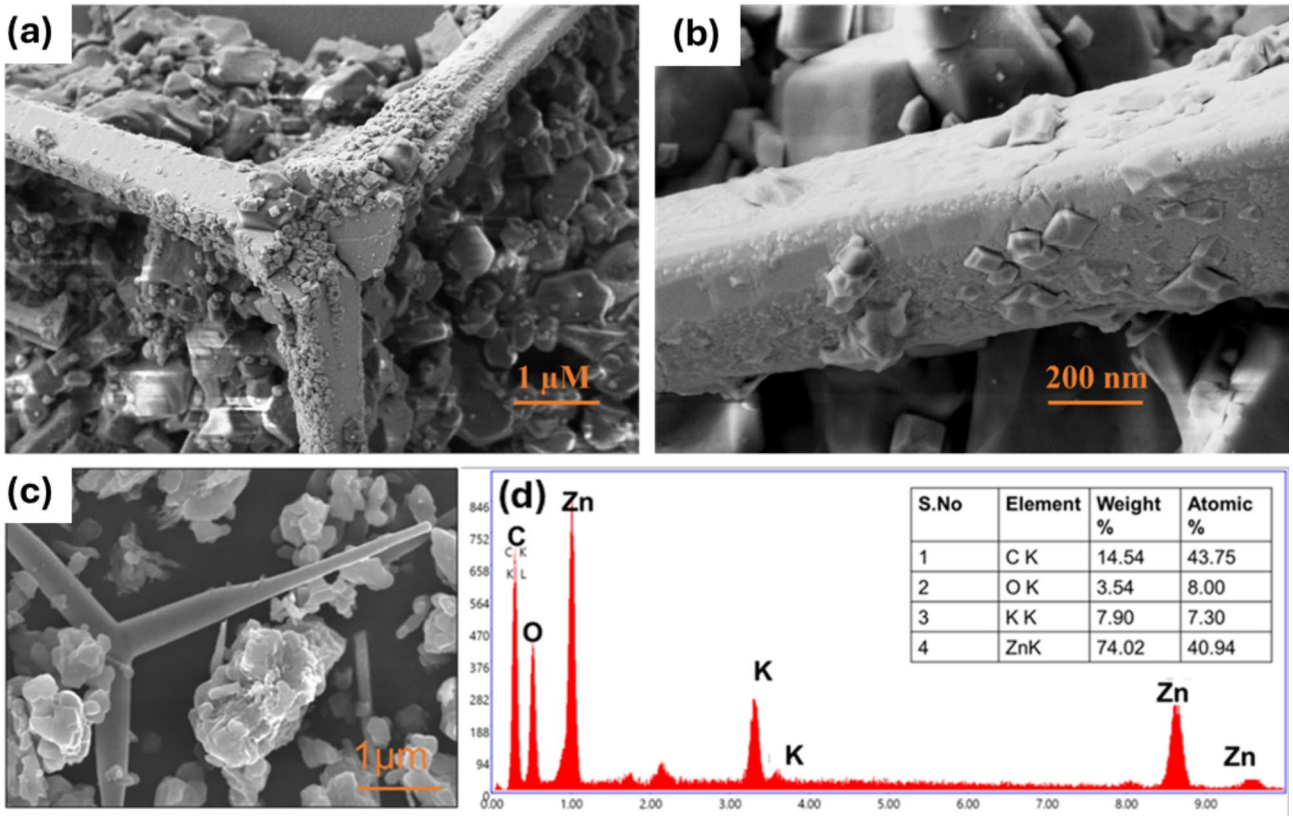

Fig. 2. SEM Image of ZnOT-K_4PTC SEM with different magnifications presenting the morphological information about the surface of the sample material (**a**, **b**,**c**) and EDX spectra of as-synthesized ZnOT-K_4PTC (**d**).

the presence of oxygen atoms that are hydroxyl groups (C-OH) bonded to carbon. Potential functional groups or surface hydroxyl groups, including those found in alcohols, phenols, or carboxylic acids, may cause this peak. The identification of oxygen atoms with more intricate bonding configurations, including those observed in carboxylic acid groups (O = C-OH), is indicated by the peak at 534 eV[44]. The four deconvoluted peaks at 284.4, 285.3, 286.9, and 288.7 eV were identified in the high-resolution C 1 s spectrum Fig. 3c as C = C, C–C, C–O, and C = O, respectively[45]. The peak intensities suggest a strong decoration of the T-ZnO surface by K_4PTC, indicating the successful hybrid formation. The discernible appearance of the C–O and C = O bonding peaks indicates that T-ZnO is significantly decorated with K_4PTC. The K2p spectra, as depicted in Fig. 3d, indicate that each K2p state was divided into two sub-peaks at 292 eV and 294.4 eV: 2p3/2 and 2p1/2 which can be ascribed to C-C and CO_3^{2-} (e.g., metal carbonates) groups. Both terms denote the K^+ state connected by smaller anions. The well-resolved sub-peaks also imply a distinct coordination environment for K^+ ions, which could play a critical role in the electronic properties of the nanohybrid. Information regarding the electronic structure and the coordination arrangement of potassium ions within the material can be obtained from the peak's positioning[46].

Electrochemical characterization of bio-nanohybrid electrode

Aptamer strands immobilized on the nanohybrid were accomplished via a single-step procedure. This results in hydrogen bonding interactions between the -NH groups of the aptamer strands and the hydroxyl (OH) groups on the surface of the nanohybrid. A kind of non-covalent interaction, hydrogen bonding occurs when another electronegative atom interacts with a hydrogen atom covalently bound to an electronegative atom, such as nitrogen (NH) or oxygen (OH). The NH constituents on the aptamer strands functioned as hydrogen bond acceptors, whereas the OH groups on the nanohybrid surface donated hydrogen bonds. Throughout the immobilization procedure, stable hydrogen bonds were formed between the two components as the OH groups on the nanohybrid reacted with the NH groups of the aptamer strands. This interaction enables the Aptamer strands to adhere to the nanohybrid's surface, thereby immobilizing them in position. The Cyclic Voltammetry measurements were performed using the DropSense µStat i-400 potentiostat, as visually depicted in Fig. 4a. The substantial decrease in peak anodic current ($_{Ipa}$) observed when carbon screen-printed electrodes were coated with ZnOT-K_4PTC nanohybrid can be expected to result from the repulsion between Methylene blue molecules and K + ions, both of which are cationic. Due to this repulsive interaction between the molecules and the nanohybrid, the peak current decreases from ~ 2.26µA to 0.7 µA. Meanwhile, the $I_{p.a.}$ was increased to ~ 19µA, after the HER-2 Aptamer immobilization onto CSPE/ZnOT-K_4PTC nano-bioelectrodes. The primary factor responsible for this increase is the groove-binding interaction between the MB redox probe and single-

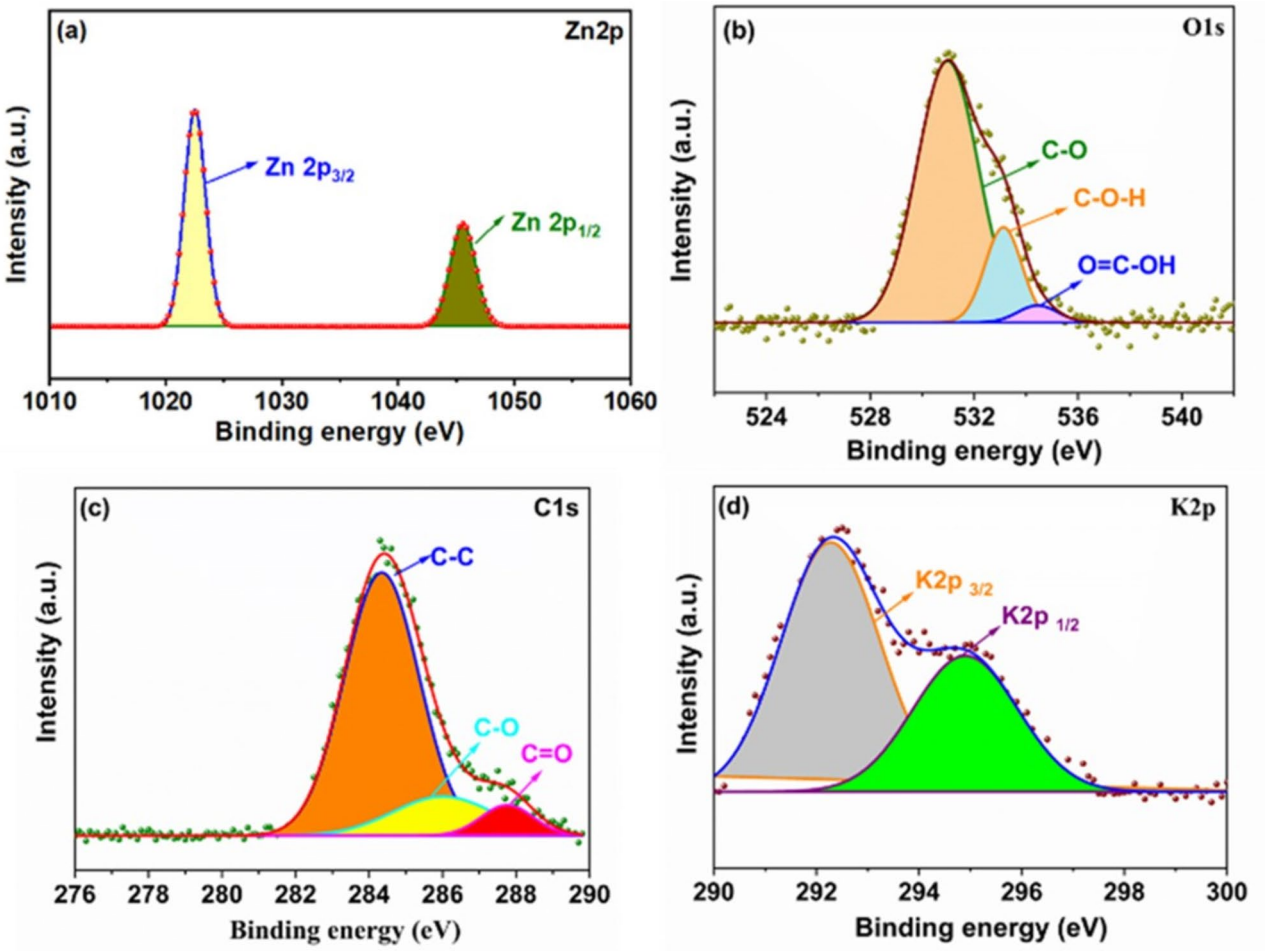

Fig. 3. XPS spectra of the synthesised ZnOT-K_4PTC (**a**) Zn2p spectrum showing the chemical state of zinc (**b**) O1s, spectrum showing oxygen species in the material, (**c**) C 1s, spectrum representing carbon bonding environments, and (**d**) K2p spectrum confirming the presence and chemical state of potassium.

stranded aptamers, which results in efficient interfacial electron transfer. The Unique behaviour observed during each phase of electrode fabrication indicates the effective development of a CSPE/ZnOT-K_4PTC/Aptamer bio-nanoelectrode. The significant potential of this electrode for detecting and analyzing breast cancer highlights the advancements in bio-nanoelectrode technology and its promising applications in medical diagnostics. The electroactive surface of the bio-nanosensors was examined by analyzing changes in current with varying scan rates (20–100 mV/s), and the corresponding cyclic voltammetry (CV) plots are displayed in Fig. 4b, demonstrate that the current profiles seem to maintain the reversible kinetics as the scan rate increasing from 20 mV/s – 100 mV/s, as proven by $I_{p.a.}/I_{pc} \sim 1$. The peak currents increase with the scan rate, as displayed in Fig. 4c, mainly exhibit a linear relationship with the half-power of the scan rate, which resembles a typical Randle 's-Sevick behaviour with diffusion-controlled kinetics. The electroactive surface region of the sensor electrode was measured to be ~0.278 mm^2 using the Randle's-Sevick Eq. 4 ref[47]. This increase in the surface area of the electrode indicates a successful modification of the electrode characteristics, providing sufficient proof that the aptamer-coated electrode was effectively modified. The high electroactive surface area of the CSPE/ZnOT-K_4PTC/Aptamer sensing electrode increased the total interface current response, providing an adequate region for examining the hybridization event. Furthermore, the Laviron plot[48] in Fig. 4d shows a change in the peak potentials as the scan rate is raised from 20 to 100 mV/s. The equations below show a linear correlation amongst log v and the peak potentials ($E_{p.a.}$ and E_{pc}).

$$\mathbf{E_{pa}} = 0.06\mathbf{log}\,(\boldsymbol{\nu}\,) - 0.27, \qquad \mathbf{R}^2 = 0.98 \tag{2}$$

$$\mathbf{E_{pc}} = -0.07\mathbf{log}\,(\boldsymbol{\nu}\,) - 0.11, \qquad \mathbf{R}^2 = 0.96 \tag{3}$$

By conducting a Comparison between these equations with the Laviron relations[49], weobtain:

$$0.06 = 2.303\boldsymbol{RT}/\,(1-\boldsymbol{\alpha}\,)\,\boldsymbol{nF} \tag{4}$$

$$-0.07 = \ 2.303\boldsymbol{RT}/\boldsymbol{\alpha}\,\boldsymbol{nF} \tag{5}$$

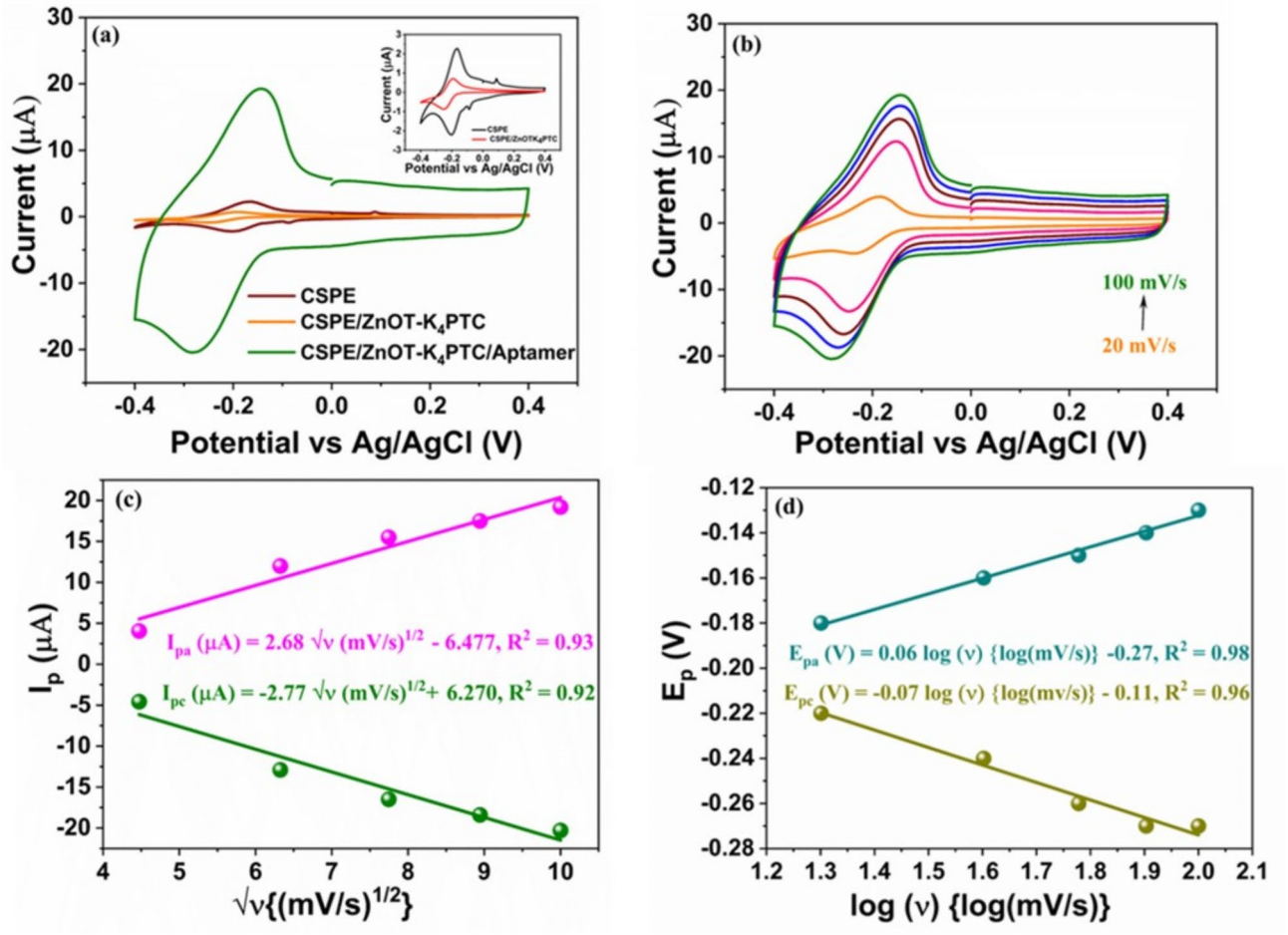

Fig. 4. (**a**) Voltametric response at various phases of electrode fabrication, (**b**) impact of scan rate on the voltammograms of the CSPE/ZnOT-K_4PTC/Aptamer sensor, (**c**) change in peak anodic and cathodic currents with varying scan rate, and (**d**) variation of peak anodic and cathodic potentials at different scan rate.

Where,

n = represents the number of electrons involved in the transfer process.

R = stands for the universal gas constant, valued at 8.314 J/K/mol.

T = is the absolute temperature measured in Kelvin.

F = denotes Faraday's constant, approximately 96,500 C/mol.

α = is the charge transfer coefficient.

The high electroactive surface area (~ 0.278 mm^2) and the average value of 'α' for CSPE/ZnOT-K_4PTC/Aptamer electrodes (0.5) are indications of an elevated degree of electron transfer, which enhances the response time of the developed sensor.

Optimization of biosensor parameters

The detailed optimization process is provided in Supplementary "Figure S1" for additional experimental results.

Analytical performance of CSPE/ZnOT-K4PTC /Aptamer sensor

The efficacy of the nano-bioelectrode to detect HER-2 recombinant protein was assessed via SWV using a frequency of 20 Hz, with a potential range of -0.6 V to + 0.2 V. A Phosphate-Buffered Saline-Methylene Blue (PBS-MB) electrolyte solution (0.1 M/100 µM, pH 7) was utilized for the experiment. The representations for the SWV profiles are shown in Fig. 5a. A reduction in peak anodic current ($I_{p.a.}$) was noted with the enhancement of HER-2 recombinant protein concentration from 1 fg/mL to 10 µg/mL. The redox process of MB, which is essential for electron transfer, is significantly inhibited when recombinant protein concentrations are increased. The electron-flow pathway is hindered due to the formation of larger hybridized complexes on the electrode surface. During DNA hybridization, these substantial complexes accumulate, creating a physical barrier that obstructs the efficient transfer of electrons. This hindrance in electron transfer results in decreased electrochemical activity, thereby affecting the overall performance of the electrode[50]. It is worth mentioning that the MB probe-mediated electrochemical reactions retain their reversibility, as evidenced by the negligible fluctuations in peak potentials and the consistent $I_{p.a.}/I_{pc}$ ratio of around 1. This observation emphasizes the sensor platform's electrochemical stability in the presence of binding events within the specified electrochemical range. The CSPE/ZnOT-K_4PTC/

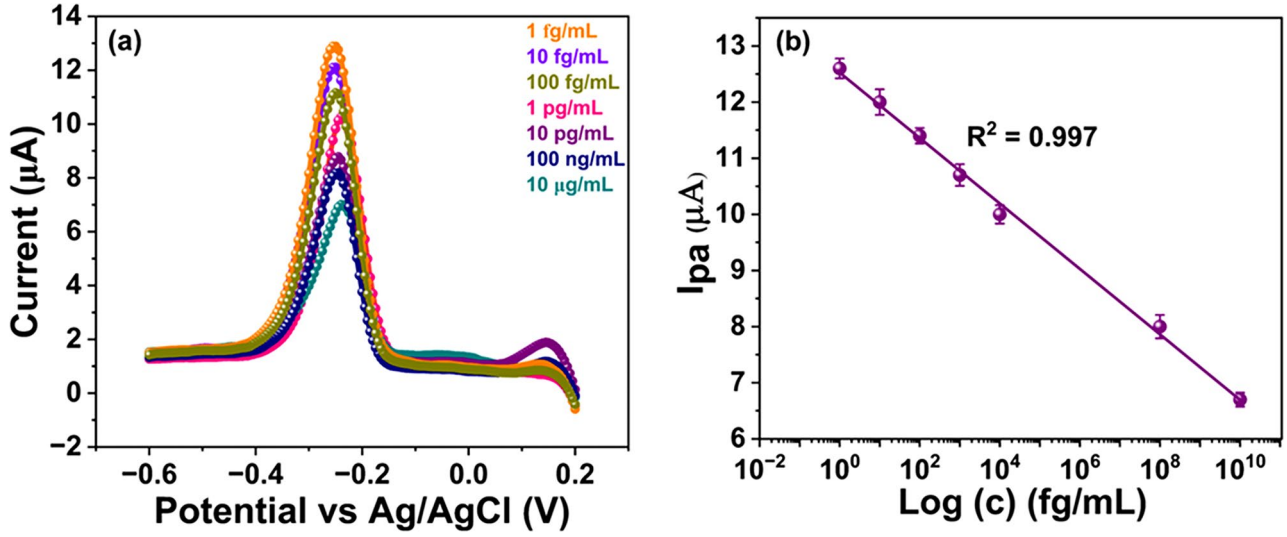

Fig. 5. (**a**) Square wave voltametric profiles obtained at various HER-2- recombinant protein concentrations within the range of 1 fg/mL to 10 µg/mL, (**b**) sensor calibration plot obtained at 0.24 V (-240 mV) within the specified concentration range.

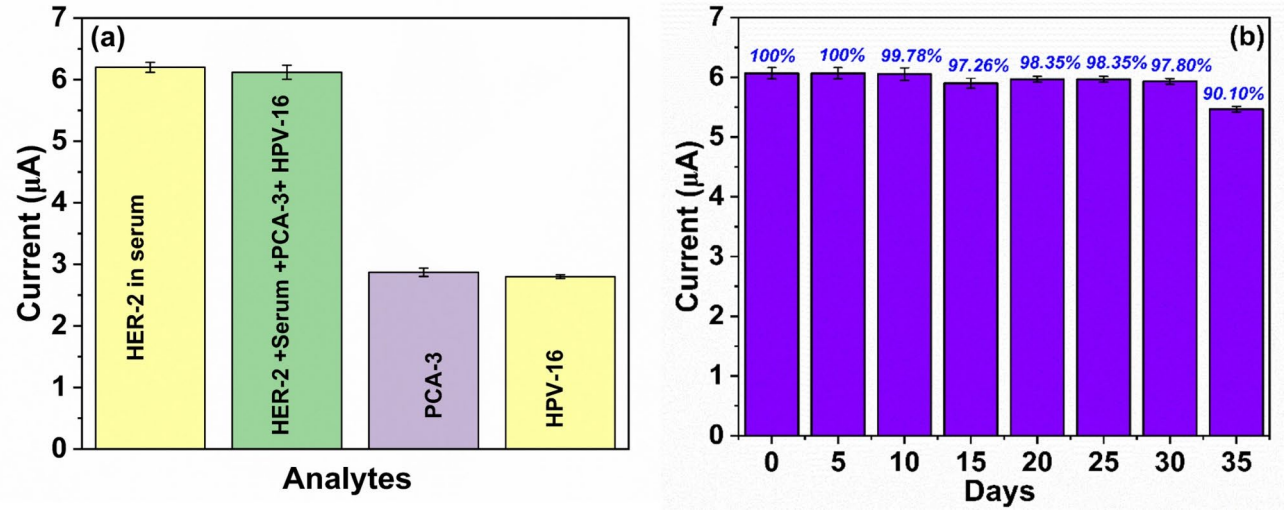

Fig. 6. (**a**) Interference and spiked serum sample study, (**b**) shelf-life study of the developed sensor over a duration of one month.

Aptasensor was calibrated to a peak anodic potential of -240 mV. The concentration of recombinant protein was shown to have a linear relationship with $I_{p.a.}$, as illustrated in Fig. 5b. As the concentration of HER-2 Recombinant protein varied from 1 fg/mL to 10 µg/mL, the current response decreased from ~ 7.0 µA to 12.9 µA, respectively. This decrease in $I_{p.a.}$ is primarily due to the formation of large complexes during DNA hybridization, which hinders electron transfer[29]. The calibration graph shows an inverse logarithmic relationship, represented by the line equation $I_{p.a.}$ (µA) = -0.583 log {c (fg/mL)] + 12.5 with an R^2 value of 0.99. The developed biosensor had a sensitivity of 2.08 µA/fg/mL /mm² and a limit of detection (LoD) of 0.58 fg/mL as determined using the 3 σ rule[51]. Table S1, please see Supplementary Information (SI), compares the key parameters of the ZnOT-K_4PTC platform with the few existing studies.

To analyse the specificity of the aptasensing platform, its efficacy was tested in spiked serum and the presence of different analytes. These analytes included HER-2 (1 fg/mL), HPV-16 (1 fg/mL), and PCA3 (1 fg/mL), which were all added individually to the detection solution. The experiments were conducted under optimum conditions, specifically using PBS/MB (0.1 M/100 µM, pH 7). The results showed that the highest peak current appeared in the presence of HER-2, as shown in Fig. 6(a). In comparison, signal intensities obtained in the presence of other interfering compounds were less than 15% of those obtained with HER-2. This indicates that the developed aptasensing platform has good selectivity towards target molecules. As shown in Fig. 6b, the stability of the aptasensing platform was evaluated over 35 days. The experiments utilized a 1 fg/mL concentration of

HER-2 recombinant protein. The results demonstrated that the anodic peak current ($I_{p.a.}$) maintained a relatively stable profile for 30 days, with variations limited to a range of 6.00 ± 5.55 µA. However, there was a marked decrease in the $I_{p.a.}$ beyond this period, indicating a significant decline in the sensor's current response. This observed pattern suggests that the developed sensor shows consistent stability and reproducibility for up to 30 days, nearly corresponding to ~ 1 month.

Figure 6a Interference and spiked serum sample study, (b) shelf-life study of the developed sensor over a duration of one month.

Conclusion

This study involved the development of a novel affordable electrochemical aptasensor designed explicitly for the initial stage screening of breast malignancy by measuring HER-2 levels. This sensor was fabricated using novel ZnOT-K_4PTC nanohybrids; K_4PTC is known for its high concentration of carboxylate groups, which are appropriate for effectively binding HER-2 Aptamer. The developed sensor exhibits remarkable linearity throughout a wide range of recombinant protein concentrations, from 1 fg/mL to 10 µg/mL. It has a LoD of 0.58 fg/mL and a sensitivity of around 2.08 µA/fg/mL/ mm^2 measured using cyclic voltametric. The designed sensor shows exceptional selectivity for HER-2 recombinant protein, with negligible variations observed in spiked serum samples. The sensing platform shows a shelf life of ~ 1 month and a quick response time of ~ 10 s, making it significant for development in detecting breast cancer. Future advancements can build on this robust platform by addressing the inherent challenges in biomolecule stability, potentially through integrating molecularly imprinted polymers (MIPs) to enhance durability and shelf life further. Exploring multiplexed biomarker detection could pave the way for comprehensive diagnostic solutions. The promising outcomes of this study establish a solid foundation for developing point-of-care diagnostic tools that can revolutionize early breast cancer detection and significantly contribute to improving global healthcare outcomes.

Methods

The experimental methods and the synthesis process of the ZnOT-K_4PTC nanohybrid is details in supplementary file. (S1) The Schematic diagram S1 in supplementary file. illustrates the details about synthesis mechanism of the ZnOT-K_4PTC nanohybrid.

Data availability

The datasets used and/or analysed during the current study will be available from the corresponding author on reasonable request.

Received: 19 October 2024; Accepted: 28 January 2025
Published online: 17 May 2025

References

1. Catalán-Gómez, S. et al. Breast cancer biomarker detection through the photoluminescence of epitaxial monolayer MoS2 flakes. *Sci. Rep.* **10**, (2020).
2. Ahirwar, R., Khan, N. & Kumar, S. Aptamer-based sensing of breast cancer biomarkers: a comprehensive review of analytical figures of merit. Expert Review of Molecular Diagnostics vol. 21 703–721 Preprint at (2021). https://doi.org/10.1080/14737159.2021.1920397
3. Bilous, M. et al. Current perspectives on HER2 testing: a review of national testing guidelines. *Mod. Pathol.* **16**, 173–182 (2003).
4. Onur, Z. & Kemal, M. Biosensors for Cancer biomarkers. *Biosens. - Emerg. Mater. Appl. (InTech*. https://doi.org/10.5772/16252 (2011).
5. Vajhadin, F. et al. Electrochemical cytosensors for detection of breast cancer cells. *Biosens. Bioelectron. vol*. https://doi.org/10.1016/j.bios.2019.111984 (2020). 151 Preprint at.
6. Núñez, C. Blood-based protein biomarkers in breast cancer. Clinica Chimica Acta vol. 490 113–127 Preprint at (2019). https://doi.org/10.1016/j.cca.2018.12.028
7. Wang, L. Early diagnosis of breast cancer. *Sens. (Switzerland)* **17**, (2017).
8. Hakimian, F. & Mazloum-Ardakani, M. Ag nanorod@PEI-Ag nanohybrid as an excellent signal label for sensitive and rapid detection of serum HER2. *Sci. Rep.* **13**, (2023).
9. Capobianco, J. A., Shih, W. Y., Yuan, Q. A., Adams, G. P. & Shih, W. H. Label-free, all-electrical, in situ human epidermal growth receptor 2 detection. *Rev. Sci. Instrum.* **79**, (2008).
10. Roy, S. et al. Design and development of a novel flexible molecularly imprinted electroanalytical sensor for the monitoring of diabetic foot ulcers. *Surf. Interfaces* **26**, (2021).
11. Bai, H., Wang, Y., Li, X. & Guo, J. Electrochemical nucleic acid sensors: Competent pathways for mobile molecular diagnostics. Biosensors and Bioelectronics vol. 237 Preprint at (2023). https://doi.org/10.1016/j.bios.2023.115407
12. Zouari, M., Campuzano, S., Pingarrón, J. M. & Raouafi, N. Determination of miRNAs in serum of cancer patients with a label- and enzyme-free voltammetric biosensor in a single 30-min step. *Microchim. Acta* **187**, (2020).
13. Nagabooshanam, S. et al. Electrochemical micro analytical device interfaced with portable potentiostat for rapid detection of chlorpyrifos using acetylcholinesterase conjugated metal organic framework using internet of things. *Sci. Rep.* **9**, (2019).
14. Fabiani, L. et al. Magnetic beads combined with carbon black-based screen-printed electrodes for COVID-19: a reliable and miniaturized electrochemical immunosensor for SARS-CoV-2 detection in saliva. *Biosens. Bioelectron.* **171**, (2021).
15. Cho, I. H., Kim, D. H. & Park, S. Electrochemical biosensors: Perspective on functional nanomaterials for on-site analysis. Biomaterials Research vol. 24 Preprint at (2020). https://doi.org/10.1186/s40824-019-0181-y
16. Yang, S. et al. Electrochemical sensor using poly-(l-cysteine) functionalized CuO nanoneedles/N-doped reduced graphene oxide for detection of lead ions. *RSC Adv.* **10**, 18526–18532 (2020).
17. Kumar, S. et al. Effect of Brownian motion on reduced agglomeration of nanostructured metal oxide towards development of efficient cancer biosensor. *Biosens. Bioelectron.* **102**, 247–255 (2018).
18. Byakodi, M. et al. Emerging 0D, 1D, 2D, and 3D nanostructures for efficient point-of-care biosensing. *Biosens. Bioelectron. X* **12**, (2022).
19. Mishra, Y. K. & Adelung, R. ZnO tetrapod materials for functional applications. Materials Today vol. 21 631–651 Preprint at (2018). https://doi.org/10.1016/j.mattod.2017.11.003

20. Modi, G. Zinc oxide tetrapod: A morphology with multifunctional applications. Advances in Natural Sciences: Nanoscience and Nanotechnology vol. 6 Preprint at (2015). https://doi.org/10.1088/2043-6262/6/3/033002
21. Sulciute, A. et al. ZnO nanostructures application in electrochemistry: influence of morphology. *J. Phys. Chem. C.* **125**, 1472–1482 (2021).
22. Luo, Q. et al. Synthesis of ZnO tetrapods for high-performance supercapacitor applications. *Mater. Lett.* **198**, 192–195 (2017).
23. Chauhan, N. et al. Zinc oxide tetrapods based biohybrid interface for voltammetric sensing of helicobacter pylori. *ACS Appl. Mater. Interfaces*. **10**, 30631–30639 (2018).
24. Zhang, Y., Liu, G. & Wu, J. Electrochemical conversion of palmitic acid via Kolbe electrolysis for synthesis of n-triacontane. *J. Electroanal. Chem.* **822**, 73–80 (2018).
25. Pourasl, M. H., Vahedi, A., Tajalli, H., Khalilzadeh, B. & Bayat, F. Liquid crystal-assisted optical biosensor for early-stage diagnosis of mammary glands using HER-2. *Sci. Rep.* **13**, (2023).
26. Dua, P., Kim, S. & Lee, D. K. *Patents on SELEX and Therapeutic Aptamers*vol. 2 (Recent Patents on DNA & Gene Sequences, 2008).
27. Huerta-Nuñez, L. F. E. et al. A biosensor capable of identifying low quantities of breast cancer cells by electrical impedance spectroscopy. *Sci. Rep.* **9**, (2019).
28. Zhang, Y. et al. An ultrasensitive dual-signal ratio electrochemical aptamer biosensor for the detection of HER2. *Colloids Surf. B Biointerfaces* **222**, (2023).
29. Rawat, R., Roy, S., Goswami, T. & Mathur, A. An electroanalytical flexible biosensor based on reduced graphene Oxide-DNA hybrids for the early detection of human papillomavirus-16. *Diagnostics* 12, (2022).
30. Rawat, R. et al. Design and development of an electroanalytical genosensor based on Cu-PTCA/rGO nanocomposites for the detection of cervical cancer. *Mater. Chem. Phys.* **295**, (2023).
31. Rakshit, T., Manna, I. & Ray, S. K. Shape controlled Sn doped ZnO nanostructures for tunable optical emission and transport properties. *AIP Adv.* **3**, (2013).
32. Burton, A. W., Ong, K., Rea, T. & Chan, I. Y. On the estimation of average crystallite size of zeolites from the Scherrer equation: a critical evaluation of its application to zeolites with one-dimensional pore systems. *Microporous Mesoporous Mater.* **117**, 75–90 (2009).
33. Park, S. J. et al. Visible-light photocatalysis by carbon-nano-onion-functionalized ZnO tetrapods: degradation of 2,4-dinitrophenol and a plant-model-based ecological assessment. *NPG Asia Mater.* **11**, (2019).
34. Gu, Z. et al. Potassium-neutralized perylene derivative (K4PTC) and rGO-K4PTC composite as effective and inexpensive electron transport layers for polymer solar cells. *Org. Electron.* **37**, 47–54 (2016).
35. Wang, Y. et al. Temperature dependent coordinating self-assembly. *Soft Matter*. **11**, 2806–2811 (2015).
36. Wang, L. et al. Coordinating self-assembly of copper Perylenetetracarboxylate Nanorods: selectively lighting up normal cells around Cancerous ones for Better Cancer diagnosis. *ACS Appl. Mater. Interfaces*. **10**, 17630–17638 (2018).
37. Knoepfel, A. et al. Development of tetrapod Zinc Oxide-based UV sensor for precision livestock farming and productivity. *Biosens. (Basel)* **12**, (2022).
38. Talakonda, P. R. & Excitation-Intensity (EI) Effect on Photoluminescence of ZnO Materials with Various Morphologies. in Luminescence - An Outlook on the Phenomena and their ApplicationsInTech, (2016). https://doi.org/10.5772/64937
39. Mishra, Y. K. et al. Versatile fabrication of complex shaped metal oxide nano-microstructures and their interconnected networks for multifunctional applications. KONA Powder and Particle Journal vol. 31 92–110 Preprint at (2014). https://doi.org/10.14356/kona.2014015
40. Yan, L., Uddin, A. & Wang, H. ZnO tetrapods: synthesis and applications in solar cells. *Nanomaterials Nanatechnol.* **5**, (2015).
41. Sonntag, S. R. et al. In Vitro evaluation of Zinc oxide tetrapods as a new material component for Glaucoma implants. *Life* 12, (2022).
42. Kim, C. H. & Kim, B. H. Zinc oxide/activated carbon nanofiber composites for high-performance supercapacitor electrodes. *J. Power Sources*. **274**, 512–520 (2015).
43. Samadi, M., Shivaee, H. A., Zanetti, M., Pourjavadi, A. & Moshfegh, A. Visible light photocatalytic activity of novel MWCNT-doped ZnO electrospun nanofibers. *J. Mol. Catal. Chem.* **359**, 42–48 (2012).
44. Na, Y., Il, Song, Y., Il, Kim, S. W. & Suh, S. J. Study on properties of eco-friendly reduction agents for the reduced graphene oxide method. Carbon Letters vol. 24 1–9 Preprint at (2017). https://doi.org/10.5714/CL.2017.24.001
45. Kumar, R., Singh, R. K., Vaz, A. R. & Moshkalev, S. A. Microwave-assisted synthesis and deposition of a thin ZnO layer on microwave-exfoliated graphene: optical and electrochemical evaluations. *RSC Adv.* **5**, 67988–67995 (2015).
46. Rajkumari, K., Das, D., Pathak, G. & Rokhum, L. Waste-to-useful: a biowaste-derived heterogeneous catalyst for a green and sustainable Henry reaction. *New J. Chem.* **43**, 2134–2140 (2019).
47. Szroeder, P. et al. Insights into electrocatalytic activity of epitaxial graphene on SiC from cyclic voltammetry and ac impedance spectroscopy. *J. Solid State Electrochem.* **18**, 2555–2562 (2014).
48. Roy, S. et al. Electrochemistry at 2D and 3D nanoelectrodes: the interplay between interface kinetics and surface density of states. *Electrochim. Acta* **477**, (2024).
49. Tang, Y. et al. Advanced batteries based on manganese dioxide and its composites. energy storage materials vol. 12 284–309 Preprint at (2018). https://doi.org/10.1016/j.ensm.2018.02.010
50. Jia, F. et al. Impedimetric aptasensor for Staphylococcus aureus based on nanocomposite prepared from reduced graphene oxide and gold nanoparticles. *Microchim. Acta.* **181**, 967–974 (2014).
51. Ding, A. X. et al. Self-assembled aggregation-induced emission micelle (AIE micelle) as interfacial fluorescence probe for sequential recognition of Cu2 + and ATP in water. *Sens. Actuators B Chem.* **255**, 440–447 (2018).

Acknowledgements

The authors would also like thank the Central Instrumentation Centre [CIC] at UPES, Dehradun [India] and the electron beamline facilities at Suranaree University of Technology [Thailand] for assisting in this research.

Author contributions

Reema Rawat: Investigation, Data curation, Formal analysis, Validation, Writing – original draft. Souradeep Roy: Methodology, Writing – review & editing, Validation. Tapas Goswami: Visualization, Supervision, Project administration, Funding acquisition. Ashish Mathur: Visualization, Supervision, Project administration, Funding acquisition. Fatemeh Sadat Mirsafi: review & editing. Mustafa Ismael: review & editing. Till Leißner: review & editing. Yogendra Kumar Mishra: review & editing. James McLaughlin: review & editing. Krishna Kant: review & editing, resource, data presentation.

Declarations

Competing interests
The authors declare no competing interests.

Ethical approval
The project is approved by research and ethical committee (Ref no. EC/NEW/INST/2022/2820), University of Petroleum and energy studies, Dehradun for:

Additional information
Supplementary Information The online version contains supplementary material available at https://doi.org/10.1038/s41598-025-88335-3.

Correspondence and requests for materials should be addressed to K.K. or A.M.

Reprints and permissions information is available at www.nature.com/reprints.

Publisher's note Springer Nature remains neutral with regard to jurisdictional claims in published maps and institutional affiliations.